ACTUATORS

Low-voltage and high-output dielectric elastomer actuators for untethered soft machines working at 200 volts

Junbo Peng[1,2]†, Jiangshan Zhuo[1,2]†, Hongcheng Qiu[3], Ofoq Normahmedov[1,2], Mengke Shi[2], Huifeng Dong[2,4], Lvting Wang[2,4], Shengchao Jiang[2,4], Jiang Zou[5], Guoying Gu[5], Tiefeng Li[3]*, Weifei Fu[6], Boyu Peng[4,7], Hanzhi Ma[2], Ye Shi[2,4,7]*

Dielectric elastomer actuators (DEAs) are promising artificial muscles featuring large actuation strains, high energy densities, and fast response speeds. However, their reliance on kilovolt-level driving voltages remains a substantial barrier to their application in untethered systems. Here, low-voltage and high-output DEAs (LVHO-DEAs) were developed by synthesizing an elastomer material—high–dielectric constant processable high-performance dielectric elastomer, with optimized stress-strain behavior and an improved dielectric constant—and by multilayering its thin films through a scalable dry-stacking process. The developed LVHO-DEAs achieved an energy density of 38.4 joules per kilogram and a power density of 452 watts per kilogram at a nominal electric field of 20 volts per micrometer without any prestretching or high-frequency resonance. Driven by LVHO-DEAs, untethered wearable devices and soft robots with different actuation mechanisms were fabricated, demonstrating effective operation at 200 volts. These findings bridge the gap between the theoretical promise of DEAs and their practical application in untethered soft systems by enabling them to serve as high-performance actuators at low driving voltages.

INTRODUCTION

Because they can become actuated under electric fields, dielectric elastomers (DEs) have been widely recognized as "artificial muscles" that show features including large actuation strains, high energy densities, fast response, and mechanical flexibility (*1*–*3*). A typical dielectric elastomer actuator (DEA) consists of a DE layer placed between two compliant electrodes. When a voltage is applied, an electrostatic force, known as Maxwell stress (p), develops between the electrodes (*4*). This stress compresses the DE film in the thickness direction and causes it to expand in area (Fig. 1A) (*5*). Assuming a free boundary approximation, the resulting thickness actuation strain S_z can be described as (*6*)

$$S_z = -p/Y' = -\varepsilon_0\varepsilon_r(V/z)^2/Y' \quad (1)$$

where ε_r is the dielectric constant of the DE material, ε_0 is the permittivity of the vacuum, V is the applied voltage, z is the film thickness, and Y' is the apparent modulus of elasticity at the actuated strain.

The electromechanical energy density (e), the amount of electrical energy converted into mechanical energy per unit volume of material delivered by the DEA during one actuation cycle, can be estimated as (*6*)

$$e = -0.5p\ln(1+S_z) = -0.5\varepsilon_0\varepsilon_r\left(\frac{V}{z}\right)^2\ln(1+S_z) \quad (2)$$

The two equations reveal that DEAs require kilovolt-level driving voltages to deliver substantial mechanical outputs given that commonly used DE materials exhibit a dielectric constant in the range of 1 to 10, a Young's modulus value on the order of hundreds of kilopascals, and film thickness ranging from tens to hundreds of micrometers (*7*, *8*). High voltages not only cause safety issues but also complicate power systems, thereby limiting DEA applications, particularly in untethered systems (*9*). Equations 1 and 2 suggest four possible strategies to reduce the driving voltage of a DEA while maintaining its actuation output: optimizing the DE stress-strain behavior, increasing the DE dielectric constant, constructing multilayered DEAs (MDEAs), and preparing ultrathin DE films. By optimizing stress-strain behavior of DE materials and enhancing their dielectric constants, they can be made to achieve high actuation performance at low electric fields. By constructing multilayered structures and using ultrathin films, the actuation output of a DEA can be scaled up while lowering the driving voltage of each single layer.

The suggested strategies have been extensively investigated in past studies. For example, DEs with high dielectric constants have been synthesized by adding inorganic additives or introducing polar groups, mechanical properties of DEs have been adjusted by controlling side chains in the DE networks, and DEAs using ultrathin films have been fabricated via layer-by-layer coating (*10*–*13*). However, these past studies indicate that adopting just one or two strategies is insufficient to develop ultralow-voltage DEAs intended for practical applications. Only a few DEAs designed for tethered systems operated in the range of 400 to 1000 V, but they exhibited low outputs (*14*–*16*), required prestretched DE films (*17*), or operated at resonant frequencies typically on the order of hundreds of hertz (*18*). A limited number of low-voltage DEAs have been used in untethered machines. Ji *et al.* reported an untethered insect robot (*19*) and an untethered haptic device operating at voltages on the order of hundreds of volts (*20*). However, those DEAs were fabricated with prestretched polydimethylsiloxane (PDMS) films, which required a

[1]College of Mechanical Engineering, Zhejiang University, Hangzhou 310000, China. [2]ZJU-UIUC Institute, Zhejiang University, Haining 314400, China. [3]Center for X-Mechanics, Department of Engineering Mechanics, Zhejiang University, Hangzhou 310027, China. [4]Department of Polymer Science and Engineering, Zhejiang University, Hangzhou 310000, China. [5]Robotics Institute and State Key Laboratory of Mechanical System and Vibration, School of Mechanical Engineering, Shanghai Jiao Tong University, Shanghai 200240, China. [6]Zhejiang University-Hangzhou Global Scientific and Technological Innovation Center, Hangzhou 311200, China. [7]MOE Key Laboratory of Macromolecular Synthesis and Functionalization, Zhejiang University, Hangzhou 310027, China.
†These authors contributed equally to this work.
*Corresponding author. Email: litiefeng@zju.edu.cn (T.L.); yeshi@intl.zju.edu.cn (Y.S.)

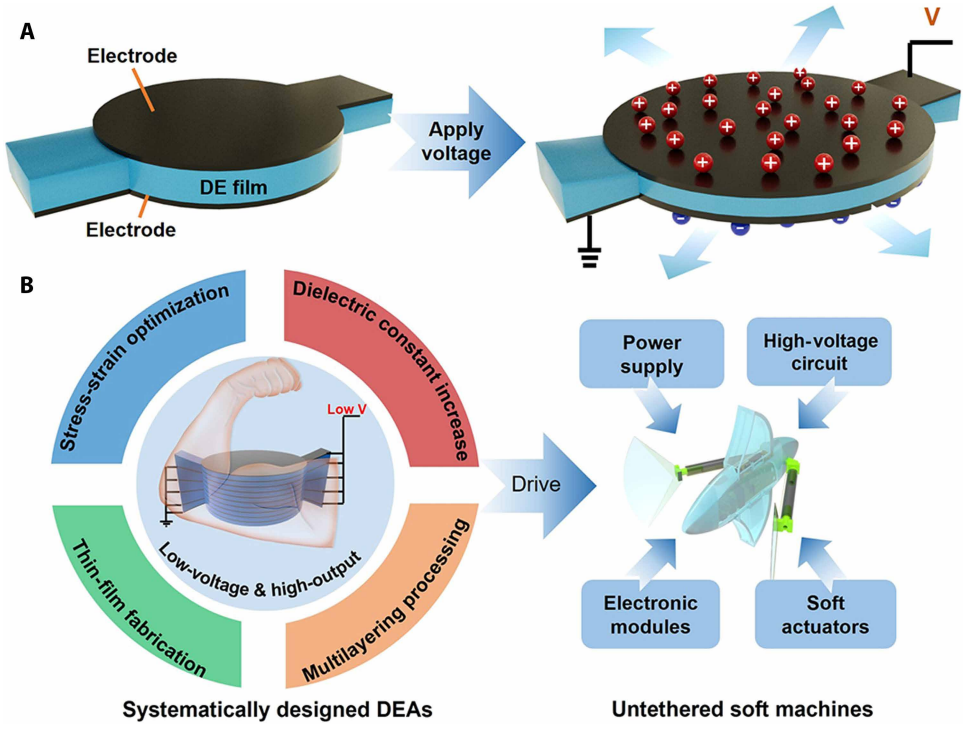

Fig. 1. High-performance DEAs for untethered soft machines. (**A**) Schematic illustration of the working mechanism of a DEA. A DEA comprises a DE film sandwiched between a pair of compliant electrodes. When a driving voltage is applied, the resulting strong electrostatic interaction between the electrodes compresses the DE film in the thickness direction and increases its area. (**B**) Strategies, including optimizing DE stress-strain behavior, increasing the dielectric constant of the DE, constructing MDEAs, and preparing ultrathin DE films, for systematically developing LVHO-DEAs to drive untethered soft machines integrated with a power supply, a high-voltage circuit, and electronic modules.

rigid frame and caused stability issues. Reducing the driving voltages to ~200 V while achieving high mechanical actuation outputs—without the need for mechanical prestretching or high-frequency resonance—is important for DEAs intended for practical applications, such as untethered soft machines and tethered systems operating at household voltages.

To develop DEAs with low driving voltages and high mechanical actuation outputs, all four strategies should be systematically implemented (Fig. 1B), which is highly challenging. A new DE material should be synthesized to simultaneously achieve optimized mechanical properties, a large dielectric constant, and high processability. A compatible multilayering method must be developed to efficiently stack these DE thin films without affecting their actuation performance. The application of low-voltage DEAs in untethered soft machines is also challenging. The DEA structure must be rationally designed to match the work mechanisms of the soft machines, and the integration of flexible and compact high-voltage and electronic modules must be achieved in miniature soft bodies.

In this study, we successfully developed low-voltage and high-output DEAs (LVHO-DEAs) by synthesizing a DE material with tunable mechanical and dielectric properties and fabricating ultrathin film–based MDEAs. When integrated with custom-designed, compact high-voltage and electronic systems, LVHO-DEAs effectively drove a variety of untethered soft machines at working voltages as low as 200 V.

RESULTS

A high-performance DE actuating at low driving electric fields without prestretching or high-frequency resonance

We first designed a DE material with a desirable stress-strain relationship and high dielectric constant to achieve high actuation performance at low driving electric fields without the need for prestretching or high-frequency resonance. Conventional methods applied to enhance the DE dielectric constant typically involve covalently grafting polar groups through complex synthesis (*21*, *22*) or incorporation of high loadings of inorganic particles, both of which can alter the mechanical and optical properties of the elastomer. For example, the addition of 5 wt % of $BaTiO_3$ nanoparticles increased the dielectric constant of the elastomer from ~5 to ~8 at 1 kHz but reduced its stretchability and optical transparency (fig. S1). We hypothesized that the bonding strength between the DE network and introduced functional moieties played a critical role in determining the material properties. Strong bonds could limit the mechanical tunability of the DE network, whereas weak bonds could lead to poor dispersion of additives. We proposed a strategy by incorporating lithium bis(trifluoromethanesulfonyl)imide (LiTFSI)—a dielectric additive with intermediate bonding strength—into a processable high-performance dielectric elastomer (PHDE) (*7*) to synthesize a high–dielectric constant PHDE (HK-PHDE) (Fig. 2A). The PHDE, featuring a bimodal network, could suppress electromechanical instability through a strain-stiffening mechanism and exhibited tunable stress-strain behavior with controlled bimodal distribution (*7*). LiTFSI could dissociate in the elastomer network and bond to polymeric chains through Li and hydrogen bonds (*23*, *24*), thereby increasing the dielectric constant without substantially changing the mechanical properties. HK-PHDE is designed to be a distinctive DE system whose stress-strain behavior and dielectric constant can be optimized by synergistically tuning the bimodal distribution and the concentration of the dielectric additive.

We next synthesized the HK-PHDE material by incorporating LiTFSI into PHDE. As shown in Fig. 2B, transparent HK-PHDE films were prepared by mixing monomers, cross-linkers, initiators, and LiTFSI to obtain a clear precursor solution, followed by blade coating and ultraviolet (UV) curing. LiTFSI demonstrated the advantage of uniform dispersion in the elastomer network, resulting in an amorphous film without phase separation, as confirmed by the small-angle x-ray scattering tests (fig. S2). It introduced firm polar groups because its cations and anions were bonded to the polymeric chains. By contrast, inorganic salts, such as LiCl, which were insoluble in PHDE, along with other organic salts that lacked strong chemical bonding to the polymer network, led to decreased dielectric strength because of the introduced mobile ions (table S1).

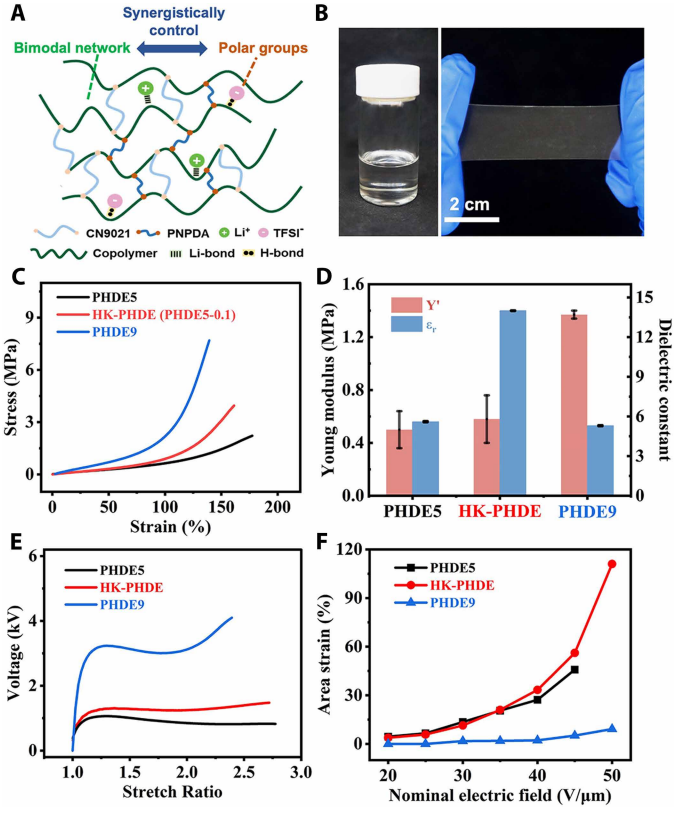

Fig. 2. Synthesis of HK-PHDE with high actuation performance at low driving electric fields. (**A**) Schematic illustration of HK-PHDE synthesis by synergistically controlling the bimodal network and bonded polar groups. CN9021 is the long-chain cross-linker, and PNPDA is the short-chain cross-linker. (**B**) Images of the precursor solution (left) and cured elastic film (right) of the HK-PHDE. (**C**) Stress-strain curves of HK-PHDE and PHDEs with no organic dielectric additives. (**D**) Comparison of Young's moduli of the HK-PHDE and other PHDEs and their dielectric constants at 1 kHz. Three samples were tested for each formulation. (**E**) Voltage-stretch curves of the HK-PHDE and other PHDEs. (**F**) Static actuation of the HK-PHDE and other PHDEs measured on a diaphragm. The film thickness was 20 μm.

Consequently, the incorporation of a small amount of LiTFSI slightly changed PHDE's Young's modulus and stretchability (Fig. 2C and fig. S3) while greatly enhancing its dielectric constant. These effects of LiTFSI were demonstrated in two other DE systems, namely, poly(lauryl arylate)–based elastomers (*11*) and butyl acrylic–based elastomer networks (fig. S4) (*25*).

Because of the high tunability of the bimodal network, we next reduced the concentration of the short-chain cross-linker propoxylated neopentyl glycol diacrylate (PNPDA) to lower the Young's modulus of elastomer and increase its stretchability. A series of PHDE samples with different amounts of PNPDA and LiTFSI were synthesized and characterized. The samples were labeled as either PHDE*x* if LiTFSI was not incorporated, with *x* indicating the weight percentage of PNPDA, or PHDE*x*-*y*, with *x* indicating the weight percentage of PNPDA and *y* indicating the weight percentage of LiTFSI. The sample formulations are listed in table S2. The measured mechanical properties and dielectric constants of the PHDE samples (fig. S5, A and B) indicated that PHDE5-0.1 was the optimal candidate for the HK-PHDE formulation, demonstrating both the highest electromechanical sensitivity and an effective electromechanical instability suppression. Further increase in the LiTFSI content led to an increase in the Young's modulus and a decrease in the actuation strain (fig. S5, C and D). HK-PHDE showed a low Young's modulus (~0.56 MPa) and high dielectric constant (~13 at 1 kHz) (Fig. 2D), with a low mechanical loss (0.23) at room temperature (fig. S6).

We next evaluated the actuation performance of HK-PHDE. The material retained the strain-stiffening behavior, which could effectively suppress electromechanical instability without the need for prestretching. According to the model developed by Zhao and Suo (*26*), the plateau observed in the voltage-stretch curve of HK-PHDE indicated electromechanical instability suppression (Fig. 2E). This electromechanical instability suppression was also verified via static actuation experiments, which revealed that the actuation strain of HK-PHDE steadily increased as the applied electric field increased, avoiding snap-through or premature failure (Fig. 2F and fig. S7). In diaphragm tests (*27*), at nominal electric fields of 35 and 50 V/μm, HK-PHDE achieved average area strains of 20 and 110%, respectively, without prestretching (Fig. 2F), demonstrating high electromechanical sensitivity (fig. S8). By contrast, with no LiTFSI addition, PHDE with 9 wt % PNPDA (PHDE9) showed much smaller strains, whereas PHDE with 5 wt % PNPDA (PHDE5) prematurely failed because of electromechanical instability. In addition, HK-PHDE demonstrated stable actuation with no detectable current leakage, and the voltage between electrodes was maintained at a constant value of 500 V, after initial charging (fig. S9).

LVHO-DEAs using multilayered HK-PHDE thin films

Although the actuation performance of HK-PHDE was improved, the mechanical output of a small-area HK-PHDE film with a thickness on the order of tens of micrometers was insufficient to drive soft machines, which required high input force or energy. The film thickness can be increased to improve the overall output for the same electric field, which, however, will lead to an enhanced driving voltage. Alternatively, MDEA fabrication can enhance the volume of active materials while maintaining the driving voltage of each layer. The selected multilayering technique should efficiently stack thin DE films while preserving their actuation performance to produce MDEAs with high overall outputs and low driving voltages (Fig. 3A).

We applied a modified dry-stacking method on HK-PHDE thin films through which the formulation and amount of adhesion layer were tuned to match the mechanical properties of HK-PHDE (*11*). The dry-stacking method allowed us to efficiently fabricate large-area HK-PHDE stacks and MDEA arrays with designed electrode patterns (Fig. 3B). It also ensured that the film thickness was uniform across the stack and that the bonding between adjacent layers was strong, as shown in Fig. 3C. Consequently, a 10-layer HK-PHDE stack exhibited a stress-strain behavior similar to that of a single-layer film (fig. S10). HK-PHDE–based MDEAs fabricated using the dry-stacking method maintained high actuation performance at low driving electric fields. In static actuation tests, at nominal electric fields of 20, 35, and 50 V/μm, their actuation area strains reached 25, 65, and 90%, respectively, with no prestretching (Fig. 3D and fig. S11). At low electric fields, the area strains of MDEAs were higher than those of single-layer HK-PHDE actuators. This difference could be attributed to the larger initial strains in single-layer films resulting from the prepressure applied during diaphragm testing (*12*). HK-PHDE–based MDEAs also exhibited fast response speed by successfully maintaining 95 and 39% of the static strain at 2 and 10 Hz, respectively (fig. S12).

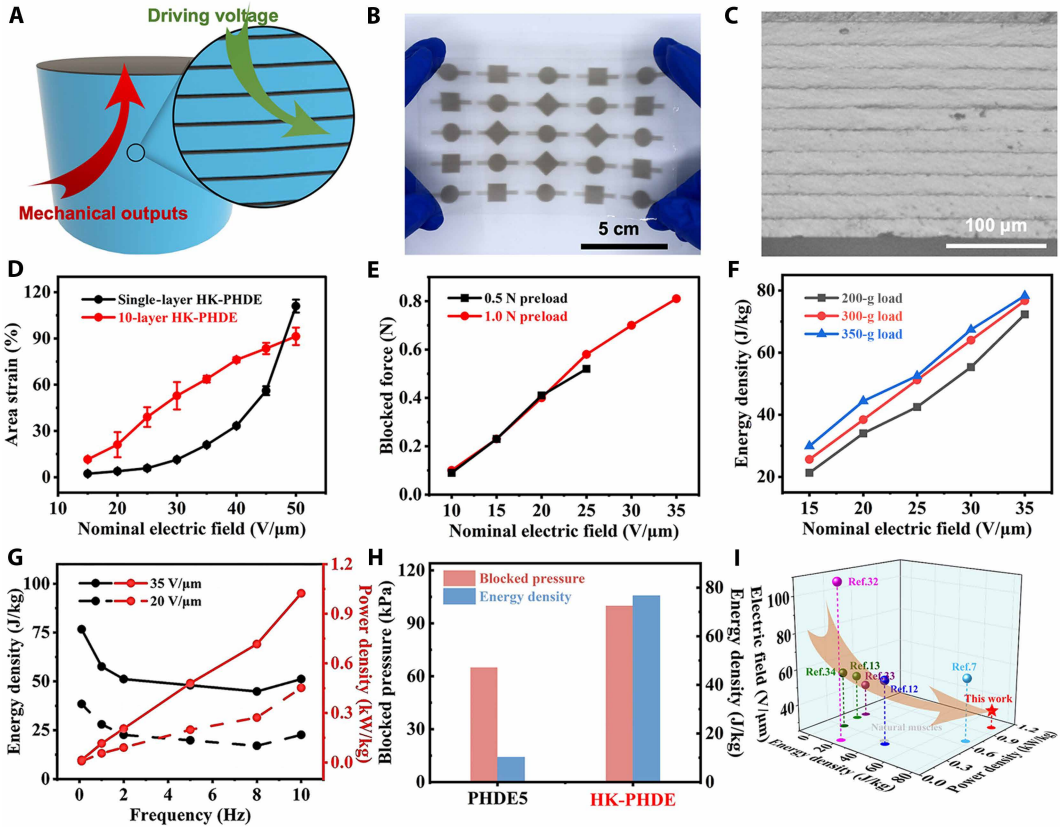

Fig. 3. Construction of MDEAs with HK-PHDE thin films. (**A**) Schematic illustration of an MDEA with scaled-up mechanical outputs and a reduced driving voltage. (**B**) A 10-layer HK-PHDE thin-film stack with an array of patterned MDEAs fabricated using the modified dry-stacking method. (**C**) Scanning electron microscopy image of the cross-sectional view of a thin 10-layer HK-PHDE film stack. (**D**) Static actuation of single-layer HK-PHDE films and 10-layer HK-PHDE stacks, measured on a diaphragm. Three samples were tested for each type of actuator. (**E**) Blocked forces of the 10-layer HK-PHDE–based MDEAs with different preloads. (**F**) Energy densities of 10-layer HK-PHDE–based MDEAs measured with different loads. (**G**) Energy densities and calculated power densities of the 10-layer HK-PHDE–based MDEAs at different frequencies under a load of 300 g. (**H**) Comparison of the blocked pressures and energy densities of the 10-layer HK-PHDE– and PHDE5-based MDEAs. (**I**) Comparison of energy and power densities of the HK-PHDE–based MDEAs and other low–electric field–driven DEAs reported in the literature.

We characterized the blocked force, energy density, and power density of HK-PHDE–based 10-layer MDEAs operating in a pure shear mode (an effective area of 40 mm by 5 mm and an active mass of ~0.044 g). In the pure shear mode, MDEAs were subjected to a uniaxial prestrain and actuated mainly along the direction of the prestrain (*27*). The setups used for the measurements are shown in fig. S13 (*28*–*31*). Under isometric conditions, at nominal electric fields of 20 and 35 V/μm, the HK-PHDE–based MDEAs subjected to a 1.0-N preload delivered output forces of 0.41 N (~51 kPa) and 0.81 N (~100 kPa), respectively (Fig. 3E). Under isotonic conditions, the energy densities of the HK-PHDE–based MDEAs were tested using different loads (Fig. 3F), and the resulting linear displacements and strains are shown in fig. S14. At nominal electric fields of 20 and 35 V/μm, the HK-PHDE–based MDEAs achieved output energy densities of 38.4 and 76.7 J/kg, respectively (Fig. 3F) when lifting a 300-g load (more than 6800 times their own weights) (fig. S15), which exceeded the mechanical capabilities of natural muscles. They also maintained output energy densities of 22.6 J/kg (at 20 V/μm) and 51.2 J/kg (at 35 V/μm) at 10 Hz, and the corresponding calculated power densities were 452 and 1024 W/kg, respectively (Fig. 3G). The force and energy outputs of the HK-PHDE–based MDEAs were higher than those of MDEAs made using PHDE5 by ~50 and 400%, respectively (Fig. 3H). The HK-PHDE–based MDEAs also exhibited much enhanced energy and power densities when compared with unmodified PHDE-based DEAs (fig. S16) (*7*). In Fig. 3I, we summarized the mechanical outputs of other low–electric field–driven DEAs reported in the literature (*7*, *12*, *13*, *32*–*34*). The arrow in the figure indicates the DEA's tendency to exhibit high energy and power densities at low driving electric fields. Our HK-PHDE–based MDEAs superseded previously reported DE-based artificial muscles along the direction indicated by the arrow.

Considering the well-maintained actuation performance of the HK-PHDE–based MDEAs at low electric fields, we controlled the driving voltage of those MDEAs by tuning their single-layer thickness values. For example, as shown in fig. S17, a maximum area strain of 118% was achieved by the 16-μm-thick HK-PHDE films under 800 V, and an area strain of 110% was achieved by the 10-μm-thick films under 500 V, both without prestretching. The driving voltage of HK-PHDE–based MDEAs could be adjusted to suit different applications. To demonstrate their actuation ability at ultralow voltages, all LVHO-DEAs implemented in the subsequent soft machines were fabricated using 10-μm-thick HK-PHDE thin films. The mentioned LVHO-DEAs were subjected to a nominal electric field of 20 V/μm while being driven at 200 V.

Untethered wearable fluidic circuits driven by roll-type LVHO-DEAs

LVHO-DEAs lead to the design and fabrication of various untethered soft machines. Wearable devices represent one of the potential applications of the LVHO-DEAs, and they place high demands on the structural flexibility of the actuators and electronic modules to achieve conformal deformation while being worn. Here, we demonstrated an LVHO-DEA–driven untethered wearable fluidic circuit used for the thermal management of hand skin. As shown in Fig. 4A, the wearable fluidic circuit comprised a silicone flow channel and reservoir, a lithium-ion battery, an electronic board, and an LVHO-DEA–based pump.

A roll-type LVHO-DEA, which exhibited high flexibility, was used as a peristaltic pump to drive the fluidic circuit (Fig. 4B). It was fabricated by stacking 10 layers of 10-μm HK-PHDE thin films and then rolling them to form a roll. When the roll-type LVHO-DEA was tested as a linear actuator, it exhibited a linear strain of 4.2% and a blocked pressure of 22 kPa at a nominal electric field of 20 V/μm (fig. S18). At 5 and 10 Hz, the output energy densities of the roll-type LVHO-DEA were 25.3 and 10.1 J/kg, respectively, under a 200-g load, and the corresponding power densities were 253 and 202 W/kg, respectively (fig. S19). The mentioned values were lower than those determined for the pure-shear mode (Fig. 3, F and G), possibly because the circumferential strain was not coupled and the linear strain was restricted by the inactive layers in the roll-type actuators. When used as a pump, the roll-type LVHO-DEA drove water at an approximate flow rate of 1.9 ml/min at 200 V and 8 Hz (Fig. 4C) and achieved a high flow rate of ~60 ml/min at 500 V and 10 Hz (fig. S20A). The corresponding specific flow rates are summarized in fig. S20B, which shows that the roll-type LVHO-DEA–based pump demonstrated superior performance compared with the electric-driven soft pumps reported in the literature (*7*, *9*, *12*, *34*–*38*). It also exhibited high stability by maintaining its initial flow rate beyond 100,000 cycles (fig. S21).

Because LVHO-DEAs could work at ultralow voltages in a range from 200 to 400 V, a highly flexible and compact electronic board, which integrated high-voltage and other electronic modules, was customized (Fig. 4D and fig. S22), thereby overcoming one of the major barriers for DEA applications in untethered systems. A picture of the fully assembled, untethered wearable fluidic circuit is shown in Fig. 4E, and a demonstration of its deployment on a human hand is shown in Fig. 4F. The roll-type LVHO-DEA and electronic board worked in highly bent states to fit the human wrist. The pump drove a continuous water flow from the reservoir into the flow channel and took about 3 min to complete a full-circulation cycle at 200 V (Fig. 4G and movie S1), which satisfied the requirements of various applications. The flow rate could be improved by increasing the driving voltage. For example, a full circulation could be run at 300 and 400 V in 36 and 10 s, respectively (fig. S23 and movie S1).

Untethered soft robotic fish driven by LVHO-DEAs

Soft robots are another important application area for DEAs (*39*–*41*) in which the structure of DEAs should be rationally designed to efficiently couple actuation with robotic motion. The structural compactness and flexibility of high-voltage and electronic systems must be further improved to reduce their constraints on robot movements. Here, we fabricated two types of untethered soft robotic fish driven by LVHO-DEAs with different actuation mechanisms.

We built a manta ray–inspired soft robotic fish driven by a planar LVHO-DEA working in pure shear mode (Fig. 5A). The planar LVHO-DEA was fabricated by stacking 20 layers of HK-PHDE thin films and assembling them in a PDMS body with minimal uniaxial prestretching (20%). Under a square wave voltage, the in-plane actuation of planar LVHO-DEA altered the bending angle of the fish body (fig. S24), thereby driving its pectoral fins to perform periodic flapping and generate the thrust required for forward propulsion. To match the size of the robotic fish, a flexible miniature high-voltage electronic board with two voltage output channels was customized (Fig. 5B and fig. S25). Figure 5C shows the assembled untethered manta ray–like soft robotic fish. The remotely activated fish achieved a swimming speed of 0.2 body length (bl)/s (1.1 cm/s) at a driving voltage of 200 V (movie S2). By contrast, a manta ray–like robotic fish driven by unmodified PHDE-based DEAs could only swim in tethered mode at a speed of 2 cm/s and a driving voltage of 700 V (*12*).

We also built an untethered sunfish-like soft robotic fish (8.5 cm long) driven by two roll-type LVHO-DEAs, as shown in Fig. 5D. The roll-type LVHO-DEA was attached with a thin polyethylene terephthalate (PET) strip, thus working in the bending mode and reaching an angle of 6.8° at a driving voltage of 200 V, as shown in Fig. 5E. It was connected with a PDMS fin and then fixed on each side of the robotic fish body (Fig. 5F). Under square wave voltages, the two roll-type actuators drove the fins to periodically flap, thereby generating forward thrust. The untethered sunfish-like soft robot achieved a swimming speed of 0.13 bl/s (1.1 cm/s) at 200 V and 2 Hz (movie S3) and 0.3 bl/s (2.6 cm/s) at 300 V (fig. S26 and movie S3). Using the same high-voltage electronic board in manta ray–like robotic fish, each roll-type LVHO-DEA was connected to one of the voltage output channels and was independently controlled. Consequently, the robotic sunfish achieved remotely controlled steering motions. Figure 5G and movie S4 show a swimming test of the robotic sunfish at 200 V, whereas Fig. 5H shows the voltage signal patterns during the test. The robotic fish began swimming forward while turning left, driven by the initial actuation of actuator B on its right side. When actuator B was remotely deactivated and actuator A on the left side was engaged, the fish took a right turn. Last, with both actuators active, the fish swam straight forward.

Soft crawling robots driven by LVHO-DEAs

Because of their high outputs at ultralow voltages without the need for prestretching, LVHO-DEAs can be integrated into various actuation mechanisms and facilitate the design of soft robotic systems. An untethered soft crawling robot was fabricated by directly dry-stacking a planar LVHO-DEA—the active component—onto a PET-based electronic board—the passive layer—and then bending the resulting assembly (Fig. 6A). The electronic board contained a miniature (2 cm–by–1.6 cm) voltage-amplifying module (fig. S27A) and a battery (1 cm by 1 cm). Figure 6B shows the crawling robot before and after bending, which indicated that dry stacking ensured firm bonding at the interface between HK-PHDE and PET films. The resulting one-piece structure was simple but efficiently integrated, using an asymmetric design to achieve out-of-plane actuation. The robot crawled at a speed of 0.33 cm/s under a driving voltage of 200 V and a 6-Hz signal (Fig. 6C and movie S5). Snapshots taken at 0 and 14 s (Fig. 6C), corresponding to the voltage-off and voltage-on states, showed the actuation-induced change in the angle between the robot leg and ground. Our LVHO-DEA–based robot showed reconfiguration capability. As shown in Fig. 6 (A and D) and movie S5, the crawling robot was reshaped by bending its leg in the opposite direction, and the robot continued to crawl at 0.45 cm/s.

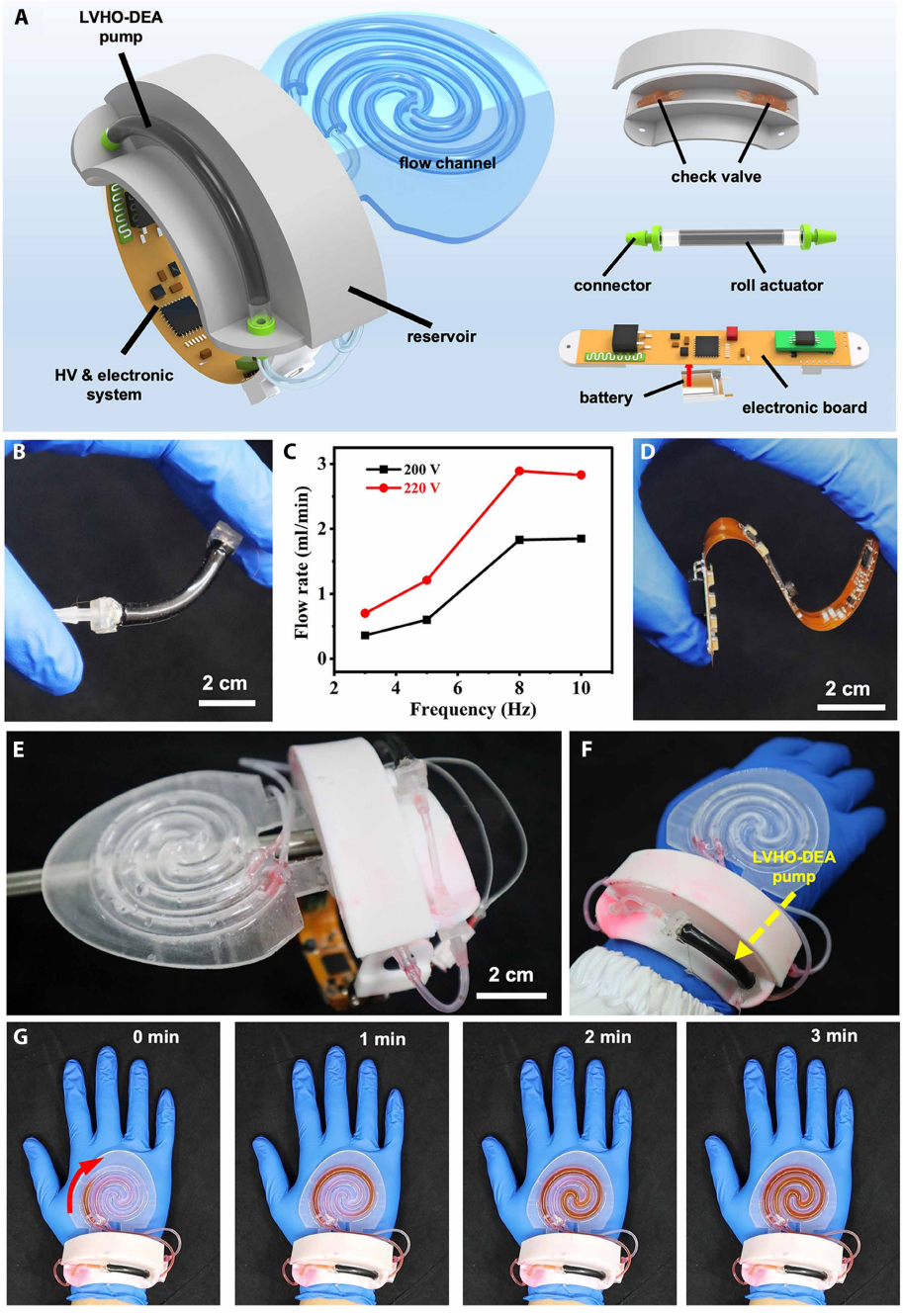

Fig. 4. An untethered wearable fluidic circuit driven by an LVHO-DEA–based pump for thermal management of the hand. (**A**) Schematic illustration of the untethered wearable fluidic circuit and its functional components. (**B**) An image of the roll-type LVHO-DEA based on HK-PHDE. (**C**) Water flow rates achieved by the LVHO-DEA–based pump at 200 and 220 V. (**D**) An image of the customized flexible miniature electronic board integrated with high-voltage and remote-control modules. (**E**) An image of the assembled untethered wearable fluidic circuit. (**F**) An image showing the untethered fluidic circuit worn on a human hand. (**G**) Snapshots of a working untethered fluidic circuit in which the LVHO-DEA–based pump drives a continuous water flow. Water is stained red for easy visualization.

We also demonstrated a crawling robot directly driven by 220-V AC, the household voltage in China, showing the potential of LVHO-DEAs for desktop robotic applications at a low cost. Similar to the untethered crawling robot, the 220 V–driven robot was made by dry-stacking a planar LVHO-DEA onto a passive PET film and then bending the assembly (Fig. 6E). When a rectified 220-V ac voltage was applied, the robot exhibited out-of-plane deformation, which drove it forward (Fig. 6F and movie S6). Figure 6G and fig. S27B show the driving circuit, comprising a 220-V ac input, a switcher, an ac-to-dc rectifier, and a remote-control module. Driven by this circuit, the 0.6-g crawling robot moved at a speed of 0.62 cm/s and maintained a speed of 0.38 cm/s while carrying a 0.4-g load (Fig. 6H).

DISCUSSION

By synergistically adopting strategies, including optimizing the stress-strain behavior of DE, increasing the DE dielectric constant, constructing MDEA structures, and using ultrathin DE films, we developed LVHO-DEAs with ultralow driving voltages and high mechanical outputs. On the material front, we synthesized a DE material, named HK-PHDE, by constructing a bimodal networked elastomer with the incorporated organic dielectric additive LiTFSI. The HK-PHDE achieved an enhanced dielectric constant (~13 at 1 kHz) and an optimized stress-strain relationship via the coordinated tuning of the bimodal distribution and dielectric additive concentration. In terms of actuator fabrication, we applied a modified dry-stacking method on HK-PHDE thin films and demonstrated that the resulting MDEAs maintained high actuation performance even at low driving electric fields. By reducing the thickness of the single-layer HK-PHDE films in the MDEAs to 10 μm, we successfully developed LVHO-DEAs operating at 200 V.

On the basis of the high actuation performance of LVHO-DEAs, we developed customized, flexible, and compact high-voltage and electronic systems and fabricated several untethered soft machines, including a wearable fluidic circuit, soft robotic fish, and crawling robots. All of the machines effectively operated at voltages as low as 200 V. LVHO-DEAs worked in diverse configurations, establishing a versatile and flexible actuation platform to unlock possibilities for untethered soft machines.

To further reduce the driving voltage, stretchable electrodes with high conductivity and ultralow stiffness should be developed because the stiff carbon nanotube (CNT) electrodes limited actuations when the thickness of the HK-PHDE films was reduced to ~5 μm (fig. S28 and movie S7). In the meantime, untethered soft machines driven by LVHO-DEAs could be further integrated with sensing, data processing, and communication modules to achieve onboard environmental perception, intelligent decision-making, and task execution with no external control.

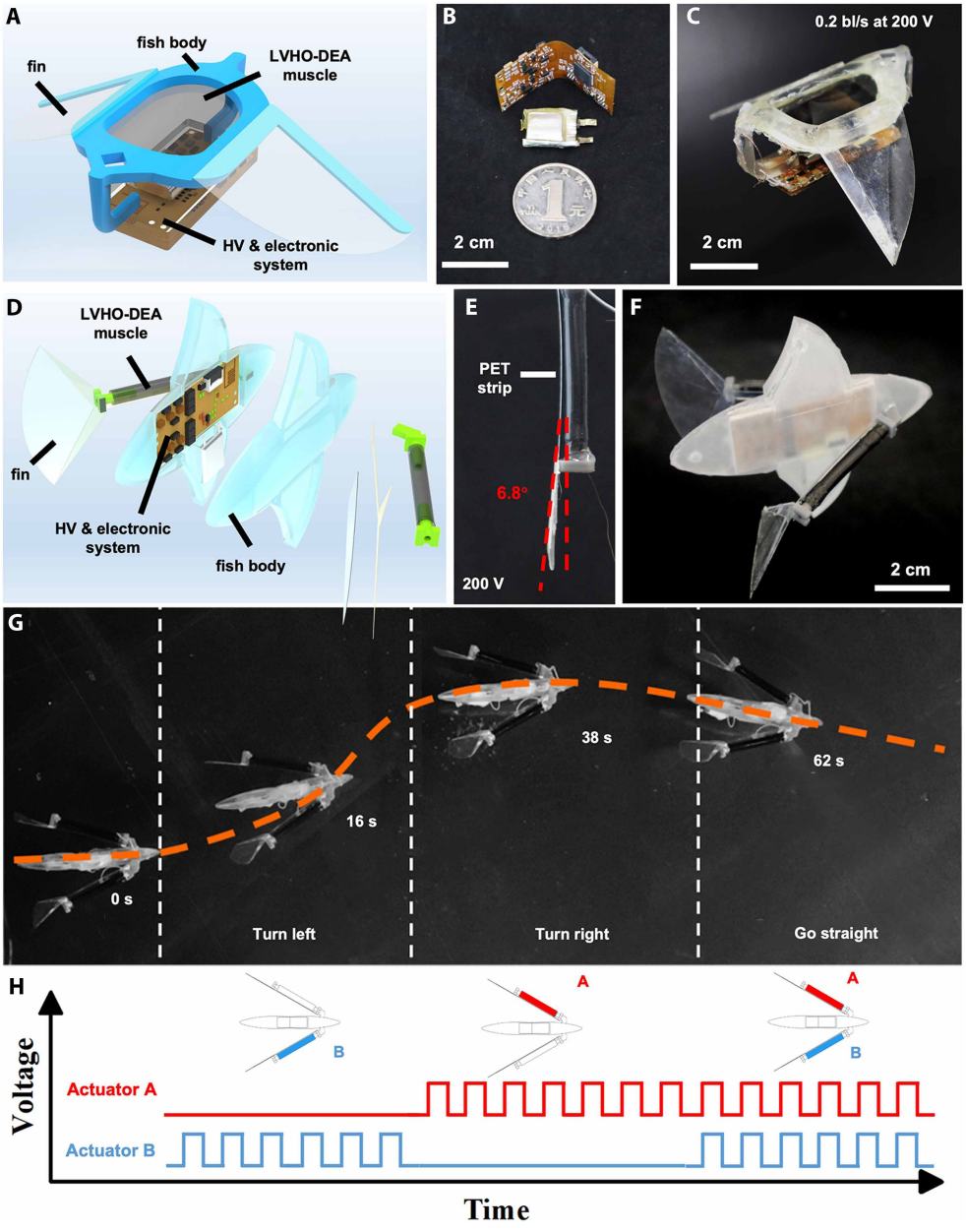

Fig. 5. LVHO-DEAs for soft robotic fish. (**A**) Schematic illustration of an untethered manta ray–like soft robotic fish driven by a planar LVHO-DEA. (**B**) An image of the customized electronic board (top), battery (middle), and a Chinese yuan coin (bottom) for comparison. (**C**) An image of the assembled untethered manta ray–like soft robotic fish. (**D**) Schematic illustration of an untethered sunfish-like soft robotic fish driven by roll-type LVHO-DEAs working in the bending mode. (**E**) Roll-type LVHO-DEA with passive strip bends at 200 V. (**F**) An image of assembled, untethered sunfish-like soft robotic fish. (**G**) Snapshots of swimming untethered sunfish-like soft robotic fish with remotely controlled steering motions. (**H**) Voltage signals applied on the roll-type LVHO-DEAs when remotely controlling sunfish-like soft robotic fish for steering motions.

MATERIALS AND METHODS

Materials

CN9021 was obtained from Sartomer Company and used with an unmodified formulation. Butyl acrylate, acrylic acid, lauryl acrylate, isobornyl acrylate, poly(acrylic acid) (PAA) solution (weight-average molecular weight ~ 100,000, 35 wt % in H_2O), benzophenone, and 2,2-dimethoxy-2-phenylacetophenone were purchased from Sigma-Aldrich. PNPDA, LiTFSI, $BaTiO_3$, and isopropyl alcohol (IPA) were obtained from Macklin company. Single-walled CNTs were purchased from Carbon Solutions Inc.

Fabrication of single-layer HK-PHDE films

The prepolymer solution was prepared by weighing the components in predetermined ratios and mixing them overnight. The PAA dilution solution (5% PAA solution in IPA) was coated on the glass as a sacrificial layer (~4 μm). The prepolymer solution was blade coated onto the glass and then UV cured two times in N_2 at 10 cm/s on a UV curing conveyor with a PM3522 curing bulb (model 3kW500ZL220V) to form the HK-PHDE film (~10, 16, and 20 μm). An acrylic frame (opening: 5 cm by 5 cm) was attached to the film with double-sided tape. After soaking in water for 1 hour, the film was peeled off from the glass and dried. The film was coated on both sides with carbon grease (NyoGel 756G, Nye Lubricants) to form compliant electrodes.

Modeling studies on the electromechanical behaviors of the prepared DEs

The model developed by Zhao and Suo (*26*) was applied to obtain the voltage-stretch (Φ-λ) curves of the prepared DEs. The Φ(λ) was derived from the following equation

$$\Phi = H\lambda^{-2}\sqrt{\sigma(\lambda)/\varepsilon} \quad (3)$$

where λ is the stretch ratio, H is the original thickness, σ(λ) is the stress-strain relationship measured from a uniaxial tensile test, and ε is the dielectric constant of the DE material.

Fabrication of MDEAs using HK-PHDE thin films

The HK-PHDE films were prepared on a 200-μm-thick PET and glass substrates after the procedure mentioned above. The HK-PHDE films on glass were trimmed to the desired shape. Then, a CNT solution (25 mg of CNTs in 4 ml of water and 36 ml of IPA) was spray coated onto the glass/DE films with paper masks to form patterned electrodes. The conductivity of the CNT electrodes was ~100 kilohms/square. The glass/DE film was thereafter sprayed with diluted DE monomer solutions (1 ml of HK-PHDE prepolymer solution in 70 ml of acetone) as a binding layer. The PET/DE film was aligned onto the glass/DE film and laminated under a pressure of 3 kg/cm^2 in vacuum. The stack was UV cured, and the PET and the stacked HK-PHDE films were peeled off from the glass

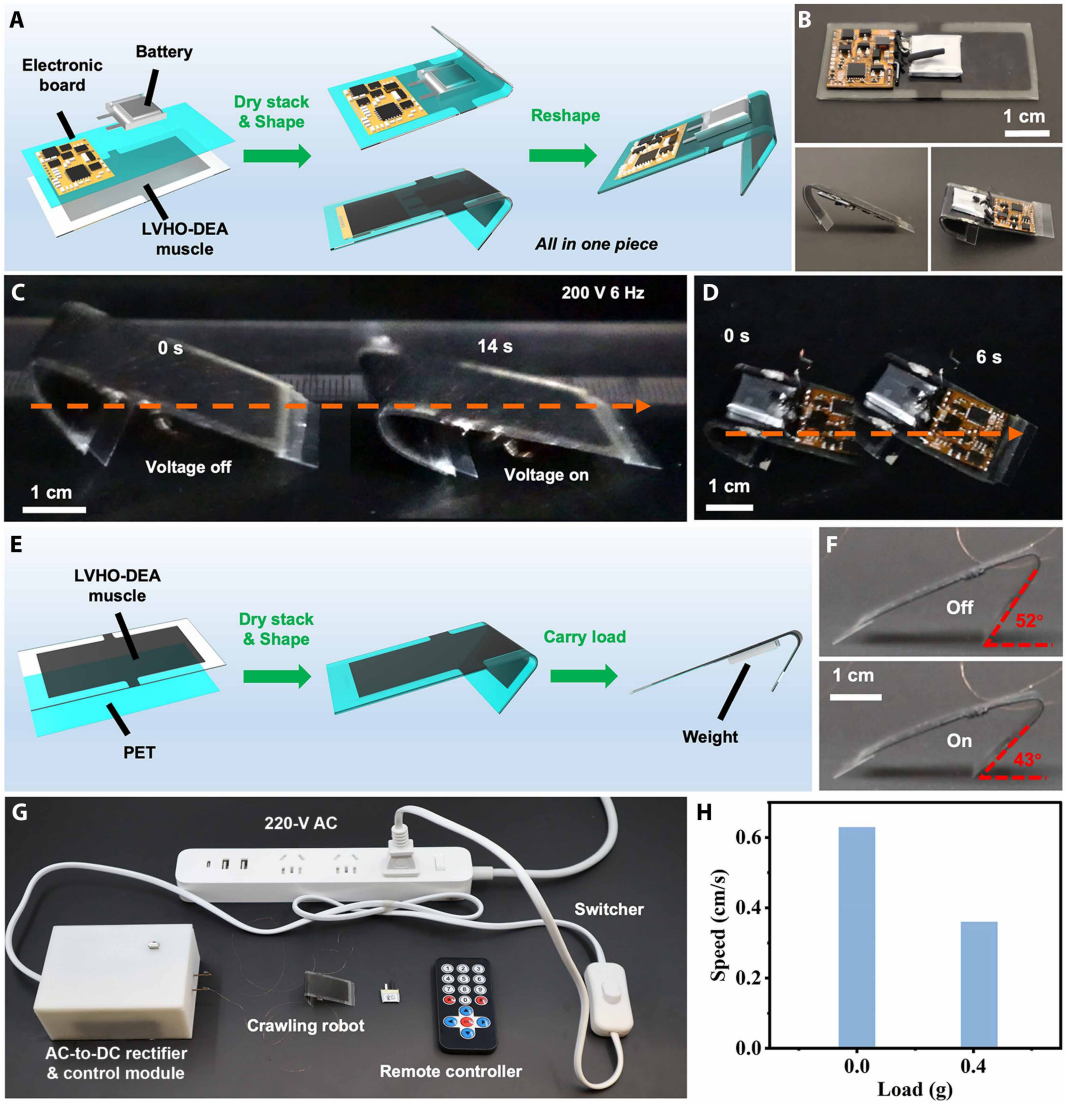

Fig. 6. LVHO-DEA–driven soft crawling robots. (**A**) Schematic illustration of the structure and fabrication of an untethered soft crawling robot based on a planar LVHO-DEA. (**B**) Images of the untethered crawling robot before shaping (top), after shaping (bottom left), and after reshaping (bottom right). (**C**) Snapshots of the untethered crawling robot in locomotion. (**D**) Snapshots of the reshaped untethered crawling robot in locomotion. (**E**) Schematic illustration of the structure and fabrication of a household 220-V AC–driven soft crawling robot based on a planar LVHO-DEA. (**F**) Household 220-V AC–driven crawling robot in its voltage-off and voltage-on states. (**G**) Driving circuit for the household 220-V AC–driven crawling robot. (**H**) Crawling speed of the household 220-V AC–driven crawling robot.

substrate. The process was repeated for each glass/DE film until the desired number of layers was achieved. Last, the stack was slowly removed from the PET at 80°C, and each side was sprayed with electrodes.

Fabrication of the roll-type LVHO-DEAs

The fabrication of the roll actuators began by stacking even layers of HK-PHDE thin films. For example, the active area of a rectangular 10-layer MDEA with a length of 90 mm and a width of 60 mm was 70 mm by 30 mm. Then, a heat-shrinkable roll with a 3-mm outer diameter was placed on a stick with a diameter of 2.8 mm. The rectangular MDEA sprayed with bonding layer solution was slowly rolled onto a heat-shrinkable roll. After the rolling process was completed, the roll actuator was UV cured and heated to remove the shrinkable roll. The ends of the roll actuator were trimmed to expose the electrodes, and carbon grease was applied to the exposed surfaces to establish electrical contact.

Fabrication of the LVHO-DEA–based soft pump

The soft pump (length, 70 mm; inner diameter, 3 mm; and outer diameter, 5 mm) was fabricated by connecting a roll-type LVHO-DEA (active length, 30 mm; inner diameter, 3 mm; and outer diameter, 5 mm) to two polypropylene connectors (length, 23 mm; inner diameter, 1.6 mm; and outer diameter, 4.7 mm) waterproofed with UV-cured PHDE.

Fabrication of the untethered manta-like robotic fish using planar LVHO-DEAs

PDMS (Sylgard 184) was used to construct the fish body (length, 60 mm; width, 45 mm; thickness, 4 mm). PDMS films (thickness,

200 μm) and a polymethyl methacrylate (PMMA) rigid frame (thickness, 1 mm) formed the wings (length, 50 mm and width, 35 mm). The wings and 3M VHB tape were fixed to the top and bottom of the body with silicone adhesive. The planar LVHO-DEA was a 20-layer MDEA (active length, 20 mm; width, 35 mm; and total thickness, ~200 μm) using HK-PHDE thin films. Thin layers of HK-PHDE were prepared on the outer surface of the LVHO-DEA for waterproofing. Last, the actuator was prestretched by 20% and assembled onto the fish body. The circuit board (length, 45 mm; width, 20 mm; and thickness, 5 mm) and battery (length, 15 mm; width, 10 mm; and thickness, 6 mm) were encapsulated in silicone and fixed to the bottom of the soft fish using two silicone connectors. The actuation of the soft robots was recorded by a Canon 60D digital camera.

Fabrication of untethered sunfish-like robotic fish using roll-type LVHO-DEAs

PDMS (Sylgard 184) was used to construct the fish body (length, 80 mm; width, 75 mm; and thickness, 8 mm), and the circuit board (length, 45 mm; width, 20 mm; and thickness, 5 mm) and battery (length, 15 mm; width, 10 mm; and thickness, 6 mm) were encapsulated in the body. PDMS films (thickness, 200 μm) and a PET frame (thickness, 200 μm) were fixed on roll actuators (active length, 30 mm; inner diameter, 3 mm; and outer diameter, 5 mm) to form the fish fins. The fins were fixed on both sides of the soft body using polypropylene connectors. The actuation of the soft robots was recorded by a Canon 60D digital camera.

Fabrication of untethered crawling robots using planar LVHO-DEAs

For the untethered crawling robot, an electronic board with a PET substrate (length, 50 mm; width, 25 mm; and thickness, 0.1 mm) was used as the passive layer. A planar LVHO-DEA with 30 layers of HK-PHDE thin films (active length, 45 mm; width, 18 mm; and total thickness, ~300 μm) was directly dry stacked on the electronic board. A battery (length, 10 mm; width, 10 mm; and thickness, 2 mm) was assembled onto the electronic board for use as a power source. For the household voltage–driven crawling robot, a PET (length, 50 mm; width, 25 mm; and thickness, 0.1 mm) was used as the passive layer, and a 20-layer LVHO-DEA (active length, 45 mm; width, 18 mm; and total thickness, ~200 μm) was dry stacked onto the PET substrate. A Canon 60D digital camera was used to record the actuation of soft robots.

Characterization of the DE materials

The small-angle x-ray scattering tests were conducted on a Xeuss 2.0 system (Xenocs SA, France) using an x-ray radiation source with an x-ray energy of 50 kV and an x-ray wavelength of 0.154 nm. The transmittance tests were performed on a UV-visible spectrophotometer (MAPADA UV-3100). The samples tested were 1 mm thick. Dynamic mechanical properties of the samples were measured using the TA Instruments RSAIII dynamic mechanical analyzer (DMA). Dynamic temperature sweep tests were performed at a heating rate of 2°C/min and a frequency of 1 Hz, covering a temperature range from −50° to 80°C. Samples measuring 8 mm in width and 120 μm in thickness (six layers) were mounted in the DMA with a 10-mm gap between the film grips.

Blocked force, blocked pressure, energy density, and power density measurements of the 10-layer MDEAs in pure shear mode

Pure-shear-type 10-layer MDEAs were fabricated with an active area measuring 4 cm in length and 0.5 cm in width. To constrain the sample edges, 170-μm-thick PET strips, also 0.5 cm wide, were bonded to the top and bottom of the MDEAs using 3M Fastbond adhesive. When measuring the blocked force, the samples were clamped on the universal tensile testing machine (CFBLSM version 0.03% F.S, China) and preloaded under isometric conditions. When the DEAs were driven by different electric fields, their deformation was fully constrained, and the maximum force was recorded as the blocked force. Blocked pressure was calculated by dividing the measured blocked force by the cross-sectional area of the 10-layer MDEAs. For energy and power density characterization, the actuators were operated under isotonic conditions with specific loads attached. A digital camera recorded the actuation strain induced by applying a voltage across the films. Given that the maximum linear strain was under 80% and the stress-strain relationship was essentially linear in this regime, the energy and power outputs were derived from the increase in potential energy of the elevated mass during MDEA contraction, which was half of one actuation cycle. The energy density (E) and power density (P) of the MDEAs were calculated using the following equations

$$E = m_1 g \Delta h / m_2 \tag{4}$$

$$P = 2E \times f \tag{5}$$

where m_1 is the mass of the load; m_2 is the mass of the active part of the actuator; g is the gravitational acceleration; Δh is the actuation displacement of the pure-shear mode DE, determined by measuring the difference between the initial height of the load when hung on the DE and the height of the load after the DE is actuated; and f is the frequency.

Permittivity measurement

Circular electrodes with a 1-cm diameter were formed by applying carbon grease onto elastomer samples of known thickness. The capacitance was then measured using a GwInstek LCR-6100 meter under a 1-V excitation across a frequency sweep of 12 to 1000 Hz. The measurements were conducted at room temperature. Relative permittivity ε was calculated as

$$\varepsilon = Ch / \varepsilon_0 A \tag{6}$$

where C is the measured capacitance, h is the thickness of the elastomer film, ε_0 is the vacuum permittivity, and A is the effective area.

Diaphragm actuation tests

To characterize the out-of-plane actuation, the elastomer films were mounted onto a PMMA diaphragm chamber featuring a 1-cm circular aperture. A constant positive air pressure of ~0.33 kPa was maintained in the chamber. The active region of the DE film was a predefined circle with a diameter of 0.9 cm before actuation. Actuation was driven by a high-voltage power supply, and the dynamic response was captured with a digital camera. The resulting actuation strain was determined by analyzing video frames with MATLAB image processing tools. The surface area (S_A) of the formed dome was calculated to quantify the strain using the following equation

$$S_A = \frac{\left(h^2 + R^2\right) - \left(h_0^2 + R_0^2\right)}{\left(h_0^2 + R_0^2\right)} \quad (7)$$

where h is the height of the dome and R is the radius. The strain values at each voltage were measured from 0.1 to 10 Hz. The nominal electric field was calculated by dividing the applied voltage by the initial thickness of the elastomer film. At least three samples were tested for each formulation.

Performance test conducted on the LVHO-DEA–based pump

Upstream and downstream check valves were placed for flow control in the LVHO-DEA–based pump. Once the fluidic system was primed with a syringe connected to a three-way stopcock, it could operate across a range of frequencies and applied voltages. During the test, the water outlet level was slightly higher than the water inlet level, and the flow rate was recorded. The blocked pressure was tested by connecting the outlet of the pump to an airtight container filled with air, and the internal air pressure was measured using a sensor. With the water pump in the container, the pressure gradually increased, and, ultimately, the pump was under the blocked condition. The initial pressure and ultimate pressure were recorded, and the blocked pressure was the difference between them.

Supplementary Materials

The PDF file includes:
Figs. S1 to S28
Tables S1 and S2

Other Supplementary Material for this manuscript includes the following:
Movies S1 to S7

REFERENCES AND NOTES

1. R. Pelrine, R. Kornbluh, Q. Pei, J. Joseph, High-speed electrically actuated elastomers with strain greater than 100%. *Science* **287**, 836–839 (2000).
2. D. M. Opris, Polar elastomers as novel materials for electromechanical actuator applications. *Adv. Mater.* **30**, 1703678 (2018).
3. C. Zhang, B. Jin, X. Cao, Z. Chen, W. Miao, X. Yang, Y. Luo, T. Li, T. Xie, Dielectric polymer with designable large motion under low electric field. *Adv. Mater.* **34**, e2206393 (2022).
4. Y. Qiu, E. Zhang, R. Plamthottam, Q. Pei, Dielectric elastomer artificial muscle: Materials innovations and device explorations. *Acc. Chem. Res.* **52**, 316–325 (2019).
5. Z. Suo, Theory of dielectric elastomers. *Acta Mech. Solida Sin.* **23**, 549–578 (2010).
6. P. Brochu, Q. Pei, Advances in dielectric elastomers for actuators and artificial muscles. *Macromol. Rapid Commun.* **31**, 10–36 (2010).
7. Y. Shi, E. Askounis, R. Plamthottam, T. Libby, Z. Peng, K. Youssef, J. Pu, R. Pelrine, Q. Pei, A processable, high-performance dielectric elastomer and multilayering process. *Science* **377**, 228–232 (2022).
8. M. Duduta, R. J. Wood, D. R. Clarke, Multilayer dielectric elastomers for fast, programmable actuation without prestretch. *Adv. Mater.* **28**, 8058–8063 (2016).
9. S. Xu, C. M. Nunez, M. Souri, R. J. Wood, A compact DEA-based soft peristaltic pump for power and control of fluidic robots. *Sci. Robot.* **8**, eadd4649 (2023).
10. C. Racles, M. Cazacu, B. Fischer, D. M. Opris, Synthesis and characterization of silicones containing cyanopropyl groups and their use in dielectric elastomer actuators. *Smart Mater. Struct.* **22**, 104004 (2013).
11. X. Dou, Z. Chen, F. Ren, L. He, J. Chen, L. Yin, Y. Luo, Z. Dang, J. Mao, Dielectric elastomer network with large side groups achieves large electroactive deformation for soft robotic grippers. *Adv. Funct. Mater.* **34**, 2407049 (2024).
12. J. Peng, J. Zhuo, H. Dong, L. Wang, S. Jiang, T. Li, Y. Shi, Dielectric elastomer actuators with low driving voltages and high mechanical outputs enabled by a scalable ultra-thin film multilayering process. *Adv. Funct. Mater.* **34**, 2411801 (2024).
13. Z. Ren, S. Kim, X. Ji, W. Zhu, F. Niroui, J. Kong, Y. Chen, A high-lift micro-aerial-robot powered by low-voltage and long-endurance dielectric elastomer actuators. *Adv. Mater.* **34**, 2106757 (2022).
14. R. Annapooranan, Y. Wang, S. Cai, Harnessing soft elasticity of liquid crystal elastomers to achieve low voltage driven actuation. *Adv. Mater. Technol.* **8**, 2201969 (2023).
15. Z. Chen, Y. Xiao, J. Fang, J. He, Y. Gao, J. Zhao, X. Gao, Y. Luo, Ultrasoft-yet-strong pentablock copolymer as dielectric elastomer highly responsive to low voltages. *Chem. Eng. J.* **405**, 126634 (2021).
16. Y. Sheima, P. Caspari, D. M. Opris, Artificial muscles: Dielectric elastomers responsive to low voltages. *Macromol. Rapid Commun.* **40**, 1900205 (2019).
17. W. Feng, L. Sun, Z. Jin, L. Chen, Y. Liu, H. Xu, C. Wang, A large-strain and ultrahigh energy density dielectric elastomer for fast moving soft robot. *Nat. Commun.* **15**, 4222 (2024).
18. H. Zhao, A. M. Hussain, M. Duduta, D. M. Vogt, R. J. Wood, D. R. Clarke, Compact dielectric elastomer linear actuators. *Adv. Funct. Mater.* **28**, 1804328 (2018).
19. X. Ji, X. Liu, V. Cacucciolo, M. Imboden, Y. Civet, A. E. Haitami, S. Cantin, Y. Perriard, H. Shea, An autonomous untethered fast soft robotic insect driven by low-voltage dielectric elastomer actuators. *Sci. Robot.* **4**, eaaz6451 (2019).
20. X. Ji, X. Liu, V. Cacucciolo, M. Imboden, Y. Civet, A. E. Haitami, S. Cantin, Y. Perriard, H. Shea, Untethered feel-through haptics using 18-μm thick dielectric elastomer actuators. *Adv. Funct. Mater.* **31**, 2006639 (2021).
21. J. V. Szczepanski, D. M. Opris, High-permittivity polysiloxanes for solvent-free fabrication of dielectric elastomer actuators. *Adv. Mater. Technol.* **8**, 2201372 (2023).
22. P. Caspai, S. J. Dunki, F. A. Nuesch, D. M. Opris, Dielectric elastomer actuators with increased dielectric permittivity and low leakage current capable of suppressing electromechanical instability. *J. Mater. Chem. C* **6**, 2043–2053 (2018).
23. B. Yiming, Y. Han, Z. Han, X. Zhang, Y. Li, W. Lian, M. Zhang, J. Yin, T. Sun, Z. Wu, T. Li, J. Fu, Z. Jia, S. Qu, A mechanically robust and versatile liquid-free ionic conductive elastomer. *Adv. Mater.* **33**, e2006111 (2021).
24. B. Yiming, S. Hubert, A. Cartier, B. Bresson, G. Mello, A. Ringuede, C. Creton, Elastic, strong and tough ionically conductive elastomers. *Nat. Commun.* **16**, 431 (2025).
25. L.-J. Yin, Y. Zhao, J. Zhu, M. Yang, H. Zhao, J.-Y. Pei, S.-L. Zhong, Z.-M. Dang, Soft, tough, and fast polyacrylate dielectric elastomer for non-magnetic motor. *Nat. Commun.* **12**, 4517 (2021).
26. X. Zhao, Z. Suo, Theory of dielectric elastomers capable of giant deformation of actuation. *Phys. Rev. Lett.* **104**, 178302 (2010).
27. F. Carpi, I. Anderson, S. Bauer, G. Frediani, G. Gallone, M. Gei, C. Graaf, C. Jean-Mistral, W. Kaal, G. Kofod, M. Kollosche, R. Kornbluh, B. Lassen, M. Matysek, S. Michel, S. Nowak, B. O'Brien, Q. Pei, R. Pelrine, B. Rechenbach, S. Rosset, H. Shea, Standards for dielectric elastomer transducers. *Smart Mater. Struct.* **24**, 105025 (2015).
28. W. Yu, W. Zheng, S. Hua, Q. Zhang, Z. Zhang, J. Zhao, W. Yuan, G. Li, C. Meng, H. Zhao, S. Guo, A prestretch-free dielectric elastomer with record-high energy and power density via synergistic polarization enhancement and strain stiffening. *Adv. Funct. Mater.* **35**, 2425099 (2025).
29. W. Yu, W. Chen, W. Yuan, G. Li, C. Meng, S. Guo, Ultrathin and highly-stable rubber electrodes based on island-bridge multi-filler conductive network for multilayer-stacked dielectric elastomer artificial muscles. *Chem. Eng. J.* **493**, 152714 (2024).
30. W. Tang, Y. Lin, C. Zhang, Y. Liang, J. Wang, W. Wang, C. Ji, M. Zhou, H. Yang, J. Zou, Self-contained soft electrofluidic actuators. *Sci. Adv.* **7**, eabf8080 (2021).
31. E. Acome, S. K. Mitchell, T. G. Morrissey, M. B. Emmett, C. Benjamin, M. King, M. Radakovitz, C. Keplinger, Hydraulically amplified self-healing electrostatic actuators with muscle-like performance. *Science* **359**, 61–65 (2018).
32. M. Duduta, E. Hajiesmaili, H. Zhao, R. J. Wood, D. R. Clarke, Realizing the potential of dielectric elastomer artificial muscles. *Proc. Natl. Acad. Sci. U.S.A.* **116**, 2476–2481 (2019).
33. Y. Chen, H. Zhao, J. Mao, P. Chirarattananon, E. F. Helbling, N. P. Hyun, D. R. Clarke, R. J. Wood, Controlled flight of a microrobot powered by soft artificial muscles. *Nature* **575**, 324–329 (2019).
34. S. Xu, Y. Chen, N.-S. P. Hyun, K. P. Becker, R. J. Wood, A dynamic electrically driven soft valve for control of soft hydraulic actuators. *Proc. Natl. Acad. Sci. U.S.A.* **118**, e2103198118 (2021).
35. W. Tang, C. Zhang, Y. Zhong, P. Zhu, Y. Hu, Z. Jiao, X. Wei, G. Lu, J. Wang, Y. Liang, Y. Lin, W. Wang, H. Yang, J. Zou, Customizing a self-healing soft pump for robot. *Nat. Commun.* **12**, 2247 (2021).
36. V. Cacucciolo, J. Shintake, Y. Kuwajima, S. Maeda, D. Floreano, H. Shea, Stretchable pumps for soft machines. *Nature* **572**, 516–519 (2019).
37. L. Wang, J. Zhuo, J. Peng, H. Dong, S. Jiang, Y. Shi, A stretchable soft pump driven by a heterogeneous dielectric elastomer actuator. *Adv. Funct. Mater.* **34**, 2411160 (2024).
38. M. Smith, V. Cacucciolo, H. Shea, Fiber pumps for wearable fluidic systems. *Science* **379**, 1327–1332 (2023).
39. G. Li, X. Chen, F. Zhou, Y. Liang, Y. Xiao, X. Cao, Z. Zhang, M. Zhang, B. Wu, S. Yin, Y. Xu, H. Fan, Z. Chen, W. Song, W. Yang, B. Pan, J. Hou, W. Zou, S. He, X. Yang, G. Mao, Z. Jia, H. Zhou, T. Li, S. Qu, Z. Xu, Z. Huang, Y. Luo, T. Xie, J. Gu, S. Zhu, W. Yang, Self-powered soft robot in the Mariana Trench. *Nature* **591**, 66–71 (2021).
40. C. Christianson, N. N. Goldberg, D. D. Deheyn, S. Cai, M. T. Tolley, Translucent soft robots driven by frameless fluid electrode dielectric elastomer actuators. *Sci. Robot.* **3**, eaat1893 (2018).
41. G. Gu, J. Zou, R. Zhao, X. Zhao, X. Zhu, Soft wall-climbing robots. *Sci. Robot.* **3**, eaat2874 (2018).

Acknowledgments: We acknowledge D. Ruan and H. Wang for valuable suggestions in designing the soft fish robotics. **Funding:** This research is supported by the National Key R&D Program of China (2024YFB4707500/2024YFB4707501), the Zhejiang Provincial Natural Science Foundation of China (LR24E030002), the National Natural Science Foundation of China (T2293720/T2293722, T2125009, and 52373254), the Zhejiang Provincial Natural Science Foundation of China Major program (ZCLZ24F0102), and "Pioneer" R&D Program of Zhejiang (2023C03007). **Author contributions:** J.P., J. Zhuo, T.L., and Y.S. conceived the concepts. J.P., J. Zhuo, and O.N. designed the experiments. J.P., J. Zhuo, H.Q., M.S., H.D., L.W., and S.J. conducted the experiments and processed the data. J.P., J. Zhuo, J. Zou, G.G., T.L., W.F., B.P., H.M., and Y.S. analyzed the results. Y.S. supervised the project. J.P., J. Zhuo, and Y.S. wrote the paper. All authors commented on the manuscript. **Competing interests:** The authors declare that they have no competing interests. **Data, code, and materials availability:** All data needed to support the conclusions of this manuscript are included in the main text or Supplementary Materials. No self-developed codes were used in this study. All materials used in this study are commercially available.

Submitted 12 May 2025
Resubmitted 27 September 2025
Accepted 21 January 2026
Published 18 February 2026
10.1126/scirobotics.ady9635

Science Robotics

Low-voltage and high-output dielectric elastomer actuators for untethered soft machines working at 200 volts

Junbo Peng, Jiangshan Zhuo, Hongcheng Qiu, Ofoq Normahmedov, Mengke Shi, Huifeng Dong, Lvting Wang, Shengchao Jiang, Jiang Zou, Guoying Gu, Tiefeng Li, Weifei Fu, Boyu Peng, Hanzhi Ma, and Ye Shi

Sci. Robot. **11** (111), eady9635. DOI: 10.1126/scirobotics.ady9635

Science Robotics (ISSN 2470-9476) is published by the American Association for the Advancement of Science. 1200 New York Avenue NW, Washington, DC 20005. The title *Science Robotics* is a registered trademark of AAAS.